CO_2 Sorption Induced Dilation in Polysulfone: Comparative Analysis of Experimental and Molecular Modeling Results

Ole Hölck,[†] Martin R. Siegert,[‡] Matthias Heuchel,[‡] and Martin Böhning*,[†]

Federal Institute for Materials Research and Testing, Unter den Eichen 87, D-12200 Berlin, Germany, and GKSS Research Center, Institute of Polymer Research, Kantstrasse 55, D-14513 Teltow, Germany

Received July 12, 2006; Revised Manuscript Received October 11, 2006

ABSTRACT: Experimental sorption and dilation data of the polysulfone/CO_2 system at 308 K and pressures up to 50 bar were measured utilizing a gravimetric sorption balance and a dilatometer based on a capacitive distance sensor. The data of this glassy polymer/gas system were subjected to a thorough kinetic analysis on the basis of a viscoelastic model, which allows the separation of the diffusive/elastic fraction of the sorption/dilation process from the slower relaxational part. The results were interpreted in terms of the common dual mode sorption model and the site distribution model of Kirchheim. Detailed atomistic packing models of the same polymer/gas system were created for two reference states with regard to concentration and swelling. The CO_2 sorption isotherms of the packing models corresponding to these two swelling states, calculated using GCMC simulations, could be combined in order to interpolate the gas uptake over the intermediate pressure range with good agreement to the experimental data. The elastic part of the gas induced dilation is successfully described by MD simulations and derived partial molar volumes are in satisfying agreement with experimental findings. Finally, the *free volume* of the packing models is probed and the obtained size distribution of the *free volume* elements is compared to the results of the analysis of experimental data according to the site distribution model.

Introduction

Amorphous polymers are widely used in applications where solubility and mobility of carbon dioxide (CO_2) in the polymeric matrix are crucial to the performance of the material. Because of its plasticizing ability, supercritical CO_2 can be used as a plasticizer in processing applications.[1] The phenomenon of penetrant induced plasticization of glassy polymers is also observed in gas separation membranes,[2] where the associated changes in the polymer structure at elevated concentrations of penetrant molecules lead to a reduction of separation performance, i.e., a decrease in permselectivity. To control the sorption and swelling behavior of glassy polymer/gas systems, a deeper understanding of these phenomena on the molecular level is necessary. Therefore, in the present work, we make an attempt to combine laboratory experiments with detailed atomistic molecular dynamic simulations and the interpretation in the framework of phenomenological models.

While molecular modeling based on common molecular mechanics and molecular dynamics (MM/MD) techniques gives the opportunity to directly observe certain properties of the polymer/gas system such as the mobility of backbone atoms or penetrants or the *free volume* distribution, established analysis methods allow an indirect determination of other properties such as the diffusion coefficient and solubility of penetrant molecules.[3] However, the time scale of such simulations is limited to a few nanoseconds, and therefore, it is not possible to directly simulate relaxations of the glassy matrix as they are observed experimentally. Experiments, on the other hand, yield results of the real macroscopic system, and although molecular details cannot be observed individually, the accumulated effects permit the analysis through models on a statistical or phenomenological basis. It is the aim of this work to survey new approaches of a combined analysis of experimental and modeling results and to establish, where possible, a convergence of boundary conditions or, alternatively, an identification and isolation of comparable aspects of these seemingly incompatible methods of research. To this effect, phenomenological models are utilized as a means of interpretation of experimental data as well as to construe modeling results and thereby putting the assumptions and implications of these models to the test.

The well-known dual mode sorption model (DM model)[4,5] is the most widely used model to describe gas sorption in glassy polymers due to its easy applicability and the ability to successfully describe sorption in a wide variety of polymer/gas systems. Although the initial assumption of two distinct penetrant populations could not be clearly confirmed,[11] the concept has proven to be flexible [6,7] and the parameters are beyond their physical interpretation a valuable means to interpolate or exchange data.[8]

Several other authors successfully developed other phenomenological models to describe or predict penetrant concentration in glassy polymers. Most of these models approach sorption from the thermodynamic point of view,[9−12] often treating the system of polymer matrix, *free volume*, and penetrants as a lattice of partly occupied sites,[13−15] extending earlier models of lattice fluids[16] by introducing order parameters that describe the nonequilibrium nature of the glassy state. The associated dilation of the polymer matrix, if explicitly considered, is in most cases treated as an overall property of the matrix, i.e., analogous to the thermal expansion coefficient, specific volume, or density.

However, the main focus of this work is to discuss the experimental results in the framework of the site distribution model (SD model) that was developed by Kirchheim.[17,18] Although this model does not incorporate relaxational swelling of the matrix, its main feature comprises the penetrant induced elastic stresses, which have been recognized by Newns.[19] Newns suggested that the second-stage sorption of vapors into glassy polymers (cf., following section) is controlled by the rates of

* Corresponding author. E-mail: Martin.Boehning@bam.de. Telephone: ++49 30 8104-1611. Fax: ++49 30 8104−1617.
[†] Federal Institute for Materials Research and Testing.
[‡] GKSS Research Center, Institute of Polymer Research.

10.1021/ma061562r CCC: $33.50
Published on Web 12/07/2006

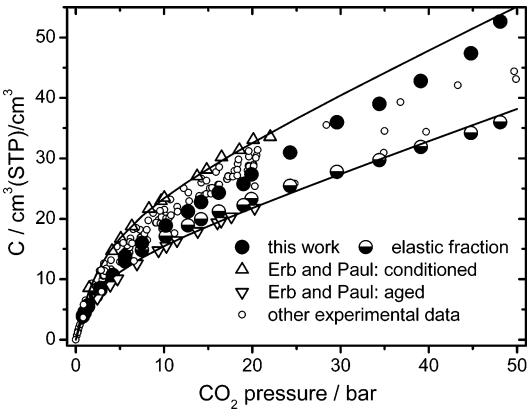

Figure 1. Concentration−pressure isotherms of the PSU−CO_2 system at 35 °C; (●, ◒): this work; (△, ▽): Erb and Paul;[25] (—): dual-mode sorption fits of ref 25; (○): data of refs 20−24,26. For the definition and derivation of the elastic fraction of this work's data, refer to the kinetic analysis section in the text.

relaxations in the polymer. The rapid initial stage of sorption, following Fickian diffusion kinetics until a quasi-equilibrium is reached, was thought to induce stresses within the polymer matrix. Limited mobility of the matrix would lead to a relaxation of the stresses and hence a decrease in chemical potential of sorbed penetrant molecules relative to the gas or vapor phase. This again would lead to a self-sustaining cycle of sorption induced stresses and relaxations which is only limited by the ability of the matrix to relax stresses and thus by the (concentration dependent) plasticizing ability of the penetrant molecule.

Following this interpretation, to understand relaxational swelling behavior, the forces that lead to the softening and subsequent relaxation need to be understood. In contrast to the thermodynamic approach, the SD model relates the distribution of sorption site volumes to a distribution of corresponding site energies. In this mechanical view, the *partial molar volume* connects the solubility of penetrant molecules to the structure of the *free volume* of the polymer matrix and thus provides a favorable basis of comparison to detailed atomistic packing models.

Because the aim of this work is also to attempt a new approach on the combined analysis of simulated and experimental data, a polymer/gas system was chosen, which shows both the sorption and dilation characteristics under consideration and which has been widely discussed in the literature, to enable classification of the data obtained in this work. As is shown in Figure 1, a number of authors have published data on carbon dioxide (CO_2) sorption in polysulfone (PSU).[20−26] Erb and Paul[25] examined polysulfone samples that were *aged* (*free volume* reduction by sub-T_g annealing) or *conditioned* (*free volume* increase by high pressure CO_2 treatment). The resulting isotherms approximately mark the lower and upper boundaries of sorption data at a temperature of 35 °C. Aside from a variety of different experimental setups, the sample prehistory, which is not always known, and the experimental time scale seem to be the main causes of the observed differences. As can be seen from Figure 1, the primary sorption data gathered in this work show that, during the time of an incremental sorption run, the state of a *conditioned* sample is reached, i.e., the measured CO_2 concentration meets the extrapolated dual mode sorption fit of ref 25, implying the sample to be conditioned during the measurement as would be expected. On the other hand, the elastic fraction (see kinetic analysis section) of this work's data seems to resemble better the behavior of the *aged* sample in ref 25.

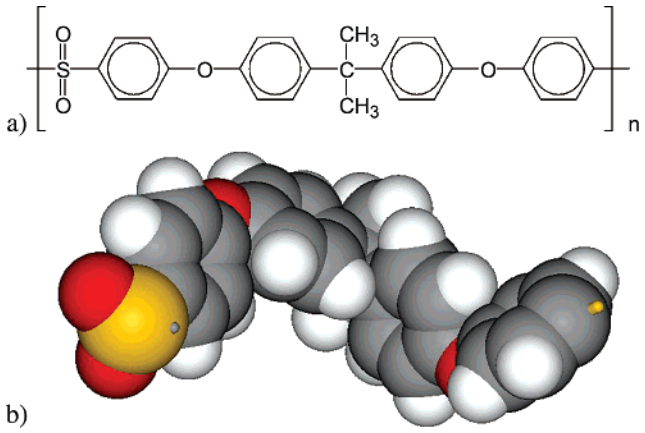

Figure 2. (a) Chemical structure of poly(sulfone) (PSU) and the corresponding equilibrated model of a single repeat unit (b). Atoms are represented by spheres of van der Waals radii: sulfur (S): yellow; oxygen (O): red; carbon (C): gray; hydrogen (H): white.

The following two sections specify the equipment used in our laboratory experiments, briefly recapitulate the applied phenomenological models and give the equations needed in the examination. Subsequently, the packing procedures for the detailed atomistic models and the respective analysis methods are shortly presented. Results of the diverse investigations and their combination are shown and discussed in detail thereafter, and the final section shortly summarizes and concludes this work.

Experimental Section

Material. Poly(sulfone) is a high-performance thermoplast used in a variety of applications and therefore readily available from a number of different suppliers; its chemical structure is given in Figure 2. In our study, Ultrason S was obtained from BASF AG, Germany, as a melt-extruded film of 100 μm thickness. DSC measurements showed noncrystallinity and a glass transition at 190 °C. Measurements in a density gradient column yielded a density of $\rho = 1.24$ g/cm^3.

Carbon dioxide (CO_2) of purity >99.995% was used as received from Air Liquide Deutschland GmbH.

Sorption. Gravimetric sorption measurements were carried out using an electronic microbalance Sartorius M25D-P from Sartorius GmbH Göttingen. Details of the setup have been described in a previous publication,[33] and only the main features should be noted here: The balance is situated in a pressure cell designed to bear pressures well over 50 bar. The temperature of the setup is held constant by an air bath at 35 ± 0.1 °C. Deviating from ref 33, data acquisition was computer aided, recording the signal of the microbalance automatically at a rate of 0.5 s^{-1}.

The film sample of uniform thickness is cut into several pieces (~10 mm × 10 mm × 0.1 mm) and put onto the balance pan inside the cell, which is then evacuated at $p < 10^{-5}$ mbar until any significant weight change has ceased. After degassing of the sample, the CO_2 pressure is increased in a series of stepwise increments, and the weight gain Δm of the sample is observed for at least 24 h at each step (Figure 3). As the effect of buoyancy is nearly instantaneous, compared to the slower kinetics of the weight gain due to sorption, it is easily eliminated from the data.

The weight gain is converted into the commonly used units of cm^3 (STP)/cm^3 (polymer) using

$$C = \frac{\hat{V}_{id}\Delta m}{\hat{M}_{CO_2}} \cdot \frac{\rho_0}{m_0} \tag{1}$$

where $\hat{V}_{id}$ is the volume of a an ideal gas at standard conditions (STP), $\hat{M}_{CO_2}$ the molar mass of CO_2, and ρ_0 and m_0 the density and mass of the polymer prior to any measurement, respectively.

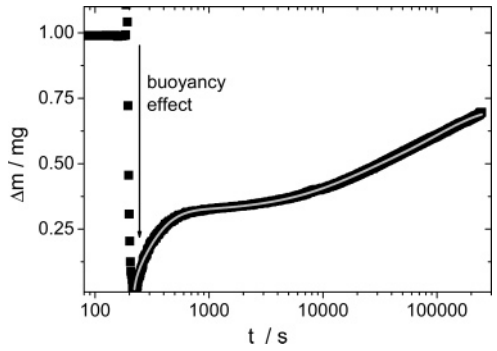

Figure 3. Representative mass uptake signal in PSU/CO_2 (■) and best fit of the viscoelastic model eq 3 (—). Pressure step 25−30 bar. The buoyancy effect is easily discernible.

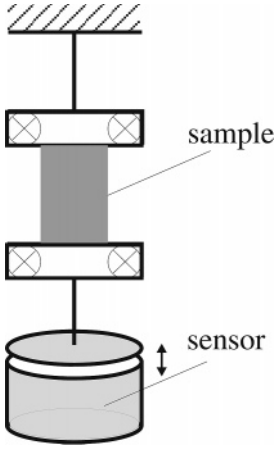

Figure 4. Principle of the dilatometer based on a capacitance sensor.

Dilation. Various techniques to measure sorptive dilation of glassy polymers are reported in the literature. While earlier methods were based on visual readouts,[27,28] more recently, induction gauges,[29,30,38] ellipsometry,[31] or image analysis[32] are utilized to monitor the swelling of polymer/gas systems. In this work, the volume changes in the sample due to sorption of gas molecules were investigated using a gas pressure dilatometer, whose principle is shown in Figure 4 and which has been described in more detail in ref 33. It is based on a capacitive distance measuring system:

A strip (~20 mm × 10 mm × 0.1 mm) of the sample film is clamped at both ends. The upper clamp is fixed to the cell wall, while at the lower end, a small metal disk is attached perpendicular to the film plane. Thus the disk is suspended freely above the capacitance sensor, serving as its counter plate. Distance changes between the two plates of this capacitor can be measured linearly within a range of 1000 μm and with an accuracy of 0.25 μm. The weight of the lower clamp and metal disk (<10 g) is not expected to significantly influence the measurement, as the exerted stress is almost 3 orders of magnitude below the yield stress of the PSU specimen.

Similarly to the sorption setup, the dilatometer is placed in a pressure cell which is held at constant temperature by an air bath. In contrast to ref 33, a second sensor has been added to the chamber with a fixed distance to its counter plate; its signal is used to eliminate the effects due to dielectric changes of the gas atmosphere.

The Labview-based software allows data acquisition rates of up to 1 s^{-1}. Following the same procedure as in the sorption measurements, after thorough degassing, the length change of the sample is recorded for a series of pressure increments, and at least 24 h observation time per step were scheduled.

Assuming isotropic swelling, the length change Δl of the sample can be easily converted to volume change ΔV using

$$\Delta V/V_0 = (1 + \Delta l/l_0)^3 - 1 \qquad (2)$$

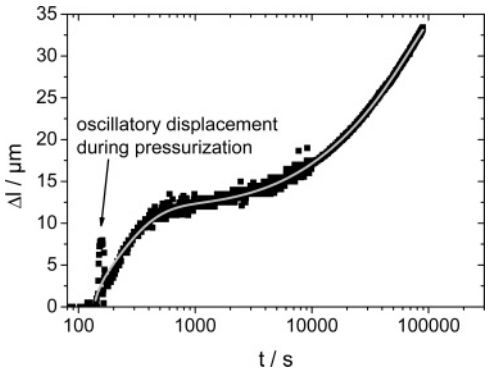

Figure 5. Representative dilation signal in PSU/CO_2 (■) and best fit of eq 3 (—). Pressure step 25−30 bar. Note that, at long observation times (>10^4 s), a lower acquisition rate allows a reduction of the oscillatory scatter through averaging of the signal over several seconds.

where l_0 and V_0 denote the initial length and volume of the sample.

Kinetic Analysis. Generally, three cases of diffusion of penetrants in glassy polymers are distinguished:[34] (1) case I or Fickian diffusion in which the rate of diffusion is much less than that of relaxation; (2) case II diffusion in which diffusion is very rapid compared with the relaxation processes; (3) non-Fickian or anomalous diffusion, which occurs when diffusion and relaxation rates are at a comparable level.

For the obtained data of CO_2 diffusion into glassy PSU at 308 K, the shape of the mass uptake curve (Figure 3) implies anomalous diffusion with a two-stage sorption process, where the initial rapid stage is controlled by Fickian diffusion, whereas the second stage is dominated by relaxational processes of the polymer matrix. The same two-stage behavior is observed for the dilation curve (Figure 5). Thus, for a detailed analysis of the kinetics of sorption and dilation, the following model function has been fitted to the sorption and dilation data, respectively:

$$X(t) = X_f \cdot f(t,D) + X_{g1} \cdot g_1(t,\tau_1) + X_{g2} \cdot g_2(t,\tau_2) \qquad (3)$$

where

$$f(t,D) = 1 - \sum_{n=0}^{\infty} \frac{8}{(2n+1)^2\pi^2} \exp\{-D(2n+1)^2\pi^2 t/d^2\} \qquad (4)$$

and

$$g_i(t,\tau_i) = 1 - \exp\{-t/(d^2\tau_i)\} \qquad (5)$$

$X(t)$ denotes the time dependent change of mass and length, respectively. The first term on the right side of eq 3 reflects Fickian diffusion kinetics into a plane sheet of thickness $d/2$ as derived by Crank[34] (eq 4). It contains the diffusion coefficient D and the diffusive fraction of the mass uptake X_f as fit parameters. Sufficient accuracy was achieved using the first three terms in the summation of eq 4 for calculations, while higher order terms were dropped for practical reasons ($n \leq 2$).

To account for non-Fickian diffusion, two exponential relaxation functions g_1 and g_2 are implemented with the relaxational fraction X_{gi} and the thickness normalized relaxation times τ_i as fit parameters. It should be noted that the normalization of the relaxation times is done for convenient comparison to the diffusion coefficient and should not imply a thickness dependence.

This approach was proposed by Berens and Hopfenberg[35] based on the treatment of solvent-vapor sorption in glassy polymers. In their model, the kinetics of vapor sorption are considered to be a linear superposition of independent contributions from Fickian diffusion and sorption controlled by relaxational processes of the polymer matrix. In general, the relaxational contribution may be written as an infinite sum of exponential functions representing first order relaxations. However, one or two relaxational terms have proven to successfully describe even complex sorption data.[35,36]

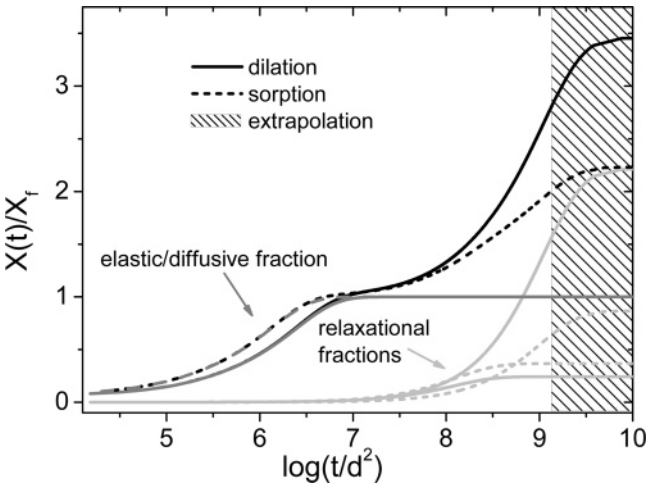

Figure 6. Mass uptake (- - -) and dilation (—) in the PSU/CO_2 system on a thickness normalized logarithmic time scale after a pressure step from 25−30 bar. A clear correlation between sorption and dilation can be seen in the kinetically separated fractions. The hatched area represents an extrapolation according to the respective best fit parameters (eq 3).

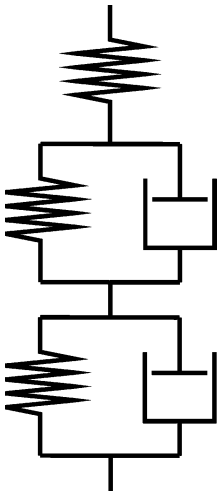

Figure 7. Spring and dashpot model to represent viscoelastic behavior.

Wessling et al.[36] applied this method to CO_2 sorption in glassy polyimides and suggested using the same kinetic model to fit the corresponding CO_2 induced dilation.

As a typical example for the behavior in the PSU/CO_2 system, Figure 6 shows mass uptake and dilation of the pressure step 25−30 bar that are shown in Figures 3 and 5, normalized to the diffusive/elastic fraction X_f and on a thickness normalized logarithmic time scale. As can be easily seen, there is a clear relation between the time scales of the different processes involved in sorption and dilation, respectively. This leads to the viscoelastic interpretation by Newns,[19] as discussed in the Introduction: eq 3 is the mathematical representation of a spring and dashpot model,[37] as shown in Figure 7.

A spring accounts for the elastic stresses imposed during the initial, rapid stage of sorption of penetrant molecules. Because this reaction of the matrix is nearly instantaneous, the slower kinetics of diffusion into the matrix is controlling the process and eq 4 applies to this elastic fraction of dilation. Two Voigt−Kelvin elements (parallel spring and dashpot) represent the viscoelastic relaxations of the polymer matrix. Their time constants τ_i, normalized to the film thickness d, are of the order $\tau_i \approx 10^8 \cdots 10^9$ s/cm^2, whereas the reciprocal diffusion coefficient is about $D^{-1} \approx 10^7$ s/cm^2 for CO_2 in PSU at 308 K at a CO_2 pressure of 30 bar (see Figure 6).

In the following, the first part, with kinetics controlled by Fickian diffusion, will be referred to as the *diffusive* fraction of sorption and elastic fraction of dilation, respectively (the terms "Fickian diffusion fraction", "diffusive fraction", and "elastic fraction" all denote the same fraction of sorption or dilation X_f, as determined by eq 3 and are used synonymously). As there is no explicit relation of the relaxation functions g_i to specific molecular motions or processes assumed here, both relaxational contributions will be discussed in terms of one relaxational fraction of sorption or dilation, meaning the sum of both relaxational functions at the end of an experimental measurement cycle.

The respective contributions for each pressure step may now be added up, resulting in separate isotherms of the diffusive/elastic and the relaxational fraction, which may be further analyzed.

Sorptive Dilation in Glassy Polymers. To describe both sorption and dilation phenomena in glassy polymer/gas systems, several models have been developed in the past.[4,11−15,17] In this work, for description of the experimental results, in addition to the most widely used dual mode sorption model (DM model), the site distribution model (SD model) has been selected because it is the only well-founded thermodynamic model, considering sorption and dilation in glassy polymers, which also provides a structural picture of the free volume distribution. The latter allows furthermore a direct comparison with the analysis of detailed atomistic molecular packing models.

Both phenomenological model approaches will be shortly described in the following. Furthermore, the relevance of the partial molar volume (pmv) and its relation to the structure of glassy polymers is emphasized.

Dual Mode Sorption model (DM). The DM model[4,5] assumes two types of sorption mechanisms in a glassy polymer. One is a simple dissolution process according to Henry's law, where the concentration of the penetrant molecules C_d depends linearly on the pressure p. The second mechanism is believed to arise from sorption into microcavities that are frozen-in below the glass transition temperature of the polymer matrix. The concentration C_h of this population of sorbed gas molecules is related to the pressure p by the Langmuir isotherm. The relation between penetrant concentration and pressure adds up to:

$$C = C_d + C_h = k_d p + \frac{C_h' b p}{1 + b p} \tag{6}$$

where k_d is the Henry's law solubility coefficient, C_h' the hole saturation constant, and b the hole affinity constant.

Site-Distribution Model (SD). The site distribution model, introduced by Kirchheim,[17] considers density fluctuations of the polymer matrix in the liquid or rubbery state above the glass transition temperature. Passing the glass transition temperature, the mobility of the polymer matrix is frozen-in, and the Gaussian distribution of this volume is preserved in the glassy state. The intermediate holes in the polymer matrix should have a Gaussian size distribution of volumes as well and are considered as sorption sites for penetrant molecules.

If a penetrant molecule, regarded as an elastic sphere of volume V_g, occupies a spherical hole in an elastic matrix (sorption site) of smaller volume V_h, it was shown that the elastic energy stored in the matrix can be expressed as[38]

$$G_{el} = \frac{2\mu_s}{3\gamma'} \frac{(V_h - V_g)^2}{V_{h0}}, \qquad V_h \le V_g \tag{7}$$

where μ_s is the shear modulus of the polymer and γ' is a constant that is related to elastic properties of the polymer and penetrant.

If the Gibbs free energy of sorption G is considered as the sum of this elastic energy G_{el} and the total of all other interactions G_r, which is assumed as equal for all sites, it was shown[17] that eqs 7 and 8 lead to a Gaussian distribution of site energies as well:

$$n(V_h) = \frac{N_0}{\sigma_V\sqrt{\pi}} \exp\left(-\frac{(V_h - V_{h0})^2}{\sigma_v^2}\right) \quad (8)$$

$$n(G) = \frac{N_0}{\sigma_G\sqrt{\pi}} \exp\left(-\frac{(G - G_0)^2}{\sigma_G^2}\right) \quad (9)$$

The widths of these distributions

$$\sigma_V = \sqrt{2kT_gV_{h0}/B}, \qquad \sigma_G = \sigma_V\frac{2\mu_s(V_g^2 - V_{h0}^2)}{3\gamma V_{h0}^2} \quad (10)$$

contain the average hole volume V_{h0} as well as the glass temperature T_g and bulk modulus B of the polymer.

Assuming similar bulk moduli for polymer and penetrant, an estimate of $N_0 = 6 \times 10^{21}$ cm^{-3} for the number of sorption sites,[17] and thermal occupancy of the sorption sites following Fermi−Dirac statistics, the penetrant concentration $C(\mu)$ and the induced volume change $\Delta V(\mu)$ can be derived:

$$C(\mu) = \int_{-\infty}^{+\infty} n(G)\, dG/(1 + \exp[(G - \mu)/kT]) \quad (11)$$

$$\frac{\Delta V(\mu)}{V_0} = \int_{-\infty}^{+\infty} \frac{(V_g - V_h(G))n(G)\, dG}{1 + \exp[(G - \mu)/kT]} \quad (12)$$

where μ is the chemical potential, which is related to the pressure via

$$\mu = \mu_0 + kT \ln[p/p_0] \quad (13)$$

with μ_0 being the standard value for $p = p_0 = 1$ bar.

The site energy of the average sorption site with volume V_{h0}

$$G_0 = G_r + \frac{2\mu_s}{3\gamma'}\frac{(V_g - V_{h0})^2}{V_{h0}} \quad (14)$$

and the width of the site energy distribution (eq 10) have been varied to obtain a best fit of eq 11 to the sorption data. The resulting values are then used as input for eq 12 to obtain a best fit to the dilation data by varying the parameter V_{h0}.

The SD model has been criticized[39] for relying on "educated guesses" concerning the shape of the distribution eq 8 and the number of sorption sites N_0. It will be shown later in this work that an analysis of the *free volume* of detailed atomistic packing models supplies valuable information about these parameters.

Partial Molar Volume (pmv). The molar volume $\hat{V}_i$ of a pure species may be defined as the ratio between its volume V_i and its quantity $\hat{N}_i$, measured in moles, at a given temperature and pressure:

$$\hat{V}_i = \left.\frac{V_i}{\hat{N}_i}\right|_{T,p} \quad (15)$$

Formally, the partial molar volume $\tilde{V}_i$ of a species i in a mixed system of volume V is defined as the variation of the volume with the amount of substance $\hat{N}_i$ of species i and constant amount of other species $\hat{N}_j$

$$\tilde{V}_i = \left.\frac{\partial V}{\partial \hat{N}_i}\right|_{T,p,\hat{N}_j} \quad (16)$$

In practice, it may be measured as the ratio of the change in the volume of the system ΔV and in the number of molecules $\Delta\hat{N}_i$ of species i:

$$\tilde{V}_i = \frac{\Delta V}{\Delta \hat{N}_i} \quad (17)$$

In liquids or rubbery polymers, the mobility of the matrix is sufficient to compensate the insertion of a penetrant molecule into a site of free volume such that the latter is kept constant. In this case, the relaxation around a penetrant molecule is complete and the pmv $\tilde{V}_i$ may be regarded as a property $\hat{V}_{g,i}$ of the penetrant phase of species i:

$$\tilde{V}_i = \hat{V}_{g,i} \quad (18)$$

In glassy polymers, the situation is different. The mobility of the matrix is limited, and therefore occupation of free volume cannot be fully compensated within reasonable time scales. The consumption of free volume by the penetrant molecules leads to a smaller partial molar volume, which must now be regarded as a property of the matrix/penetrant system. A mechanical interpretation of this phenomenon is provided by Eshelby:[40] The volume change $\Delta\hat{V}$ of an elastic continuum containing a spherical hole of volume $\hat{V}_h$, upon occupation of this hole with an elastic sphere of volume $\hat{V}_{g,i} \geq \hat{V}_h$, is given by

$$\Delta\hat{V} = \text{const}\cdot(\hat{V}_{g,i} - \hat{V}_h) = \tilde{V}_i \quad (19)$$

where const = 1 if penetrant and matrix have the same elastic properties. The partial molar volume $\tilde{V}_i$ therefore reveals information about the structure of the *free volume*, provided that the penetrant phase volume $\hat{V}_{g,i}$ is known and the matrix can be regarded as an elastic medium.

The site distribution model arises from this very picture, ascribing the distribution of site energies G to their elastic part G_{el} (eq 7), resulting from a size distribution of holes (eq 8). Consequently, the dilation (eq 12) is expressed as a summation of the misfit between all penetrant molecules and the occupied sorption sites (eq 19).

For convenience, the index i will be dropped in the following where the molar volume (in liquids or rubbers) $\hat{V}_g$ and the partial molar volume $\tilde{V}_p$ refer to the penetrant species CO_2. For an overview over selected notations used in this work, see also the Appendix.

Atomistic Packing Models. *Modeling Details.* For the molecular simulations described in detail in the following paragraphs, the Insight II (4.0.0p), Cerius^2, as well as the Materials Studio (3.2) software of Accelrys, Inc. (San Diego, CA), was used. Amorphous polymer packing models were constructed using the Theodorou−Suter method[41,42] as implemented in the Amorphous_Cell module;[43] MD simulations were performed with the Discover engine using the COMPASS force field;[44,45] for the Gusev−Suter calculations (transition state theory),[46−48] the programs GSnet and GSdiff were used. Grand canonical Monte Carlo (GCMC) simulations of sorption isotherms were realized with the Solid_Sorption module of the Cerius^2 package of Accelrys. The Insight II and Cerius^2 software modules were run on SGI Octane workstations, while the Materials Studio software was used on PC hardware as well as on an 42 Opteron processor Linux server. MD simulation runs were performed with Discover on all three platforms.

Amorphous atomistic packing models have been prepared for pure PSU at 308 K and a bulk pressure of 1 bar. These "unswollen" models are called *PSU*. Additional packing models have been prepared for the swollen state of a CO_2/polymer system, corresponding to the maximum gas pressure in our experiments of 50 bar. For the polymer chain of 94 repeat units, i.e., 5078 atoms, the respective loading, taken from the sorption experiment, corresponds to 80 CO_2 molecules, which have to be packed in addition to the chain into the simulation box. Therefore, these packing models are named in this publication *PSU80*. To obtain reasonable statistics, three packing models were created for each state (i.e., *PSU* and *PSU80*); all subsequent quantitative analyses of these models were then obtained as a mean value over the respective packing models. Table 1 summarizes the necessary data derived from combined sorption and dilation experiments, which specify the specific two "states" observed in the experiment that represent the basis for the packing models.

Table 1. Experimental Values Used to Specify the Simulated Packing Models Named in the First Column

polymer/name of state	p(CO_2) [bar]	C(CO_2) [cm^3(STP)/cm^3]	C(CO_2) [mol/mol(r.u.)]	dilation dV/V	density polymer [g cm^{-3}]	density packing[a] [g cm^{-3}]
PSU	0[b]	0.0	0.000	0.00	1.240	1.240
PSU80	50	53.4	0.85	0.067	1.162	1.260

[a] Target density of the packing model including the CO_2 molecules. [b] Bulk pressure of 1 bar.

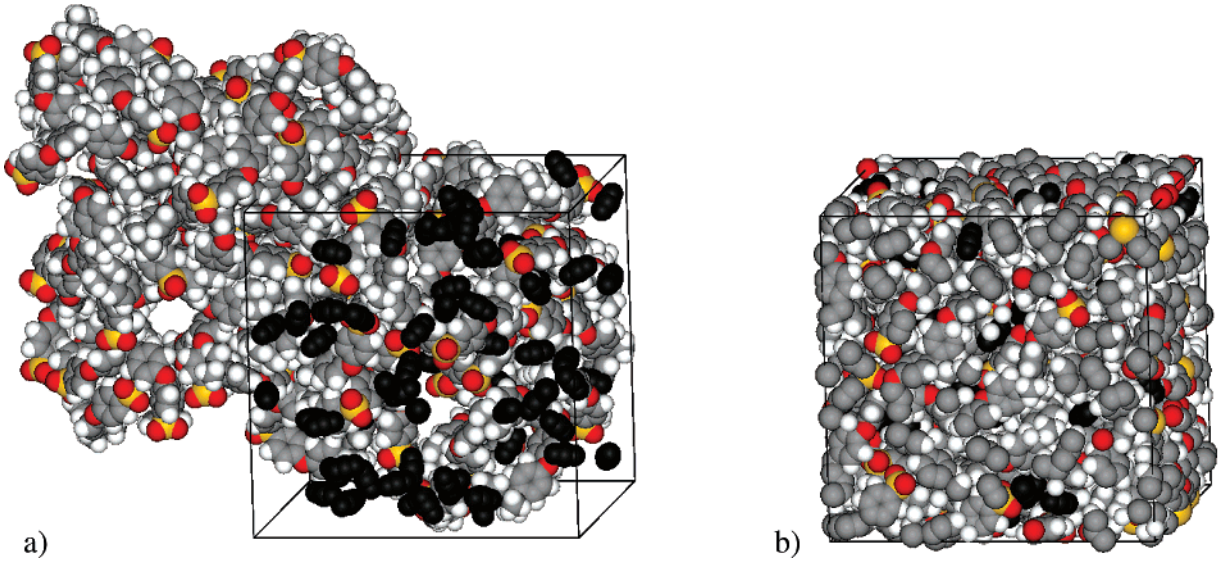

Figure 8. Single packing model for swollen polysulfone at 50 bar CO_2 pressure and 308 K (*PSU80*) in its representation as molecule chain containing 94 monomer units as depicted in Figure 2b (a) and as one simulation cell with three-dimensional periodic boundary conditions (3D-PBC) applied (b). Edge length of the simulation cell is 39.3 Å; CO_2 is displayed as a triatomic molecule in dark gray.

The densities in the last right column of Table 1 represent the target densities for the gas/polymer models. For the swollen and unswollen state of the polymer, three independent atomistic bulk models were realized. The details of the preparation of such atomistic packing models for the swollen state with respect to experimental sorption and dilation data is described in a recent publication [49] for the systems PES/CO_2 and PSU/CO_2. It should be noted that the swollen state for PSU at 50 bar in that publication corresponds to the older experimental sorption measurement,[33] with a lower sorption value (and different dilation value), and accordingly to only 55 CO_2 molecules per polymer chain of 94 repeat units.

The applied basic techniques of packing and equilibration (MM and MD) are completely described elsewhere.[3,49−51] However, a summary of the specific approach applied here to obtain the respective models will be given in the following. For the initial packing of swollen PSU models, a polymer chain was grown under periodic boundary conditions at 308 K and at a density of about 10% of the experimental value in a simulation box, where 400 CO_2 molecules were already distributed at random as obstacles to avoid packing artifacts, such as ring catenations, of the growing chain. For the growing of the chain the Theodorou−Suter method was used, as mentioned above. Then, in this "initial packing", CO_2 molecules were deleted randomly until the CO_2 concentration was adjusted to the experimental value. With a longer set of successive MD simulations, a compression and stimulated annealing of the initial packing was carried out until (with additional *NVT* and finally *NpT*-MD simulations) well-equilibrated packing models had been obtained that showed stable volume fluctuations under the experimental pressure (e.g., 50 bar for *PSU80*, see Figure 8) at a density close enough to the given experimental value. (In molecular dynamics simulations, an NVT-MD refers to an MD simulation at constant number of particles (atoms) *N*, volume of the simulation cell *V*, and temperature *T*, whereas in an *NpT*-MD, the pressure *p* is held constant instead of the volume.) By removing all CO_2 molecules from such a final model without readjusting the volume, models were derived that contained only the polymer matrix. These models were named *PSU80m*. They were later utilized to characterize the free volume distribution of the swollen state. Models for the "pure" (unswollen) polymer state *PSU* were built by deleting all CO_2 from the initial packing and subsequent equilibration and thereby adjusting the volume until the target density was reached and stable under *NpT*-MD runs.

Analysis Methods and Tools. *Size Distribution of the Free Volume.* Several definitions of free volume in glassy polymers are employed in the literature,[49] depending on the method of evaluation or the subject under investigation. In this work, the accessible free volume based on the insertion of a test particle is used. To estimate the size distributions of free volume elements (FVEs), a recently developed computer program[50] was applied to validated packing models. The free volume is derived by the superimposition of a fine grid over the cubic packing model. At every grid point, a hard sphere is inserted as a test particle. If the test particle overlaps with any atoms of the polymer matrix, which are also represented by hard spheres of van der Waals radii, the grid point is classified as "occupied". If there is no overlap, the grid point is considered as "free" and contributes to the free volume. Neighboring free grid points are collected into groups that represent individual holes. The grouping is done in two ways. In the first approach (named *V*_connect), affiliation to a group is defined through next neighborship: every point of a group has at least one next neighbor that is also member of this group. This approach identifies holes, which may be of complex shape and of large volume. In a second approach (named *R*_max) for every free grid point, the distance to the nearest matrix atom is determined. By calculation of the gradient, the grid points are assigned to the nearest local maximum in this distance. The *R*_max approach may divide larger free volume regions of elongated or highly complex shape into smaller, more compact regions. Originally introduced to match better the situation in positron annihilation lifetime spectroscopy experiments (PALS; for a more detailed discussion in this context, see ref 49; for PALS data on PSU, see refs 52,53 and for a study relating PALS with the site distribution model, see ref 54) where the positronium probe can obviously not completely sample very large holes of complex topology, the second approach also seems more adequate to depict the environment of a sorbed molecule: An oblong hole that is constricted at some point would be regarded as a single hole by

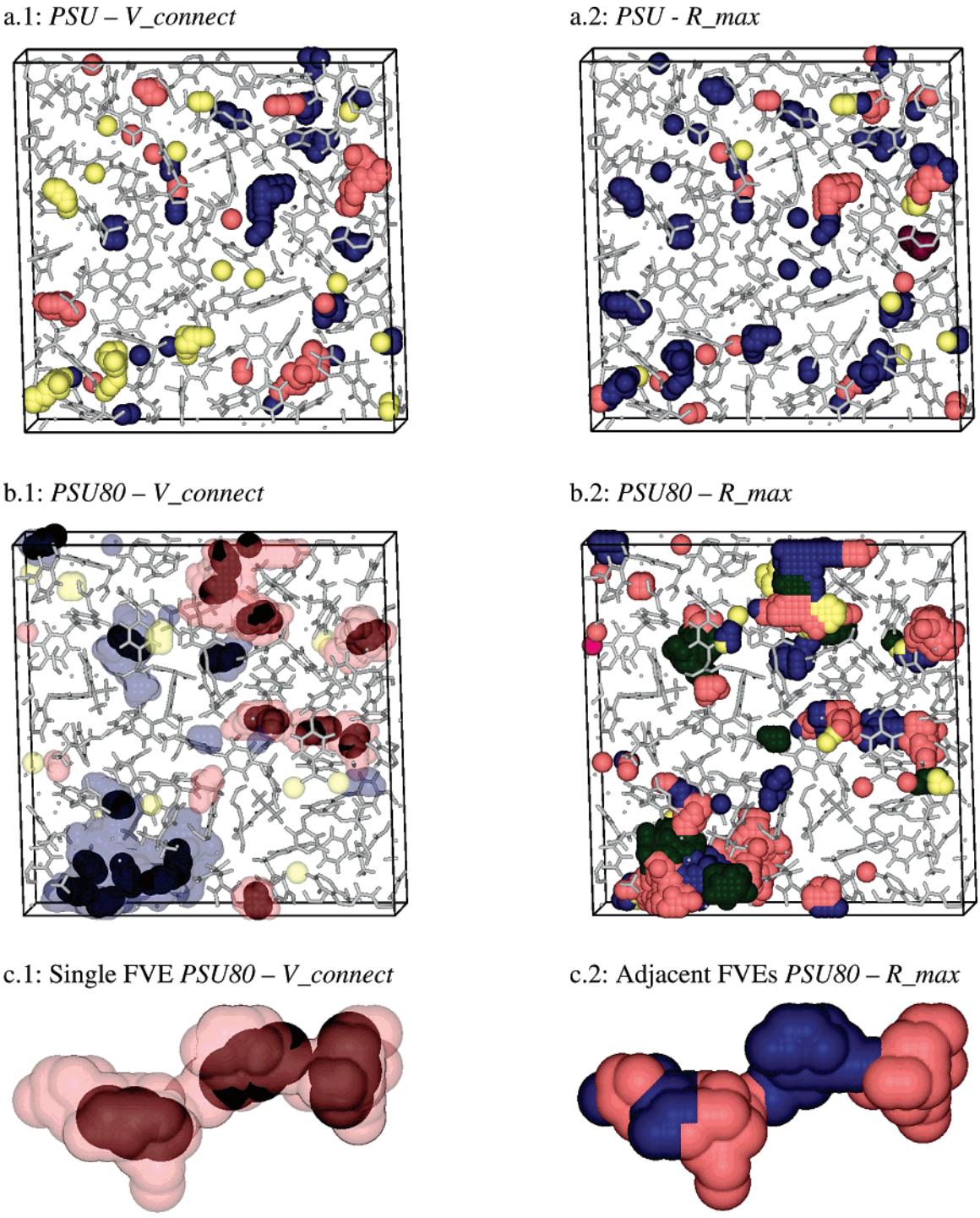

Figure 9. Visualization of free volume elements (FVEs) present in slices of 8 Å taken from a packing model of nonswollen polysulfone (*PSU*, a) and of swollen polysulfone (*PSU80*, b). Free grid points are represented by a probe-sized sphere and colored according to their interconnectivity as defined by the *V*_connect (1) and the *R*_max method (2) for better contrast. The FVEs of *PSU80* according to the *V*_connect method (b.1) are represented by their surfaces and the CO_2 molecules (dark-gray triatomic molecules) are included to show their location within the FVEs. Matrix atoms and bonds are represented as sticks (light gray) to get a better view at the FVEs. Figure c.1 shows a single FVE, containing three CO_2, as detected by the *V*_connect method in comparison to the same FVE analyzed by the *R*_max approach (c.2).

the *V*_connect method. However, a penetrant molecule would have to jump an energy barrier to pass this bottleneck and therefore "see" two separate sorption sites. By defining a hole according to the *R*_max method, this separation would be recognized.

To visualize the free volume obtained by these methods, it does not suffice to display the simulation cell as a whole (Figure 8b) because the matrix molecules obstruct the view and the great number of holes interfere with each other if displayed together. To get a better impression, the simulation cell is cut into slices of about 8 Å thickness. Figure 9 shows the centerpiece of one unswollen packing model (*PSU*) and of one swollen model (*PSU80*). For better viewing, matrix atoms are displayed in "stick style". At free grid points, a sphere of test particle size is displayed and colored according to group affiliation for clarity, if necessary. It should be noted that, due to the slicing process and to periodic boundary conditions, some matrix atoms as well as FVEs appear fragmented or continue on the opposite side.

The subdivision of sites by the *R*_max method compared to the *V*_connect method can best be seen for the FVEs of the swollen model (*PSU80*) in Figure 9b: in Figure 9b.1, the FVEs contained

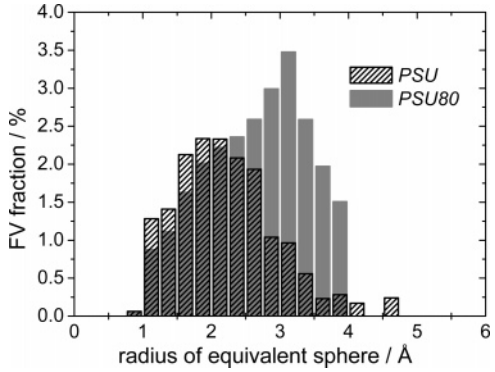

Figure 10. Size distribution of the fractional *free volume* of the unswollen (*PSU*) and swollen (*PSU80*) packing models as detected by the *R*_max method.

in a single slice taken from the center of a *PSU80* packing model are shown represented by their surfaces. Partial transparency of these surfaces allows seeing the CO_2 molecules at their respective locations inside the cavities. In Figure 9b.2, the same cavities are represented by solid spheres colored according to the *R*_max analysis. Here the subdivision of connected free volume regions into individual sorption sites can clearly be seen. Although some penetrants seem to cluster inside the two especially large cavities, the *R*_max method in Figure 9b.2 reveals the separation (in terms of local constrictions) of connected "free" grid points into smaller groups forming sorption sites. The relevance of the *R*_max method to the detection of sorption sites becomes especially obvious if the FVEs containing CO_2 are enlarged and viewed individually (Figure 9c).

To quantify the volume for each definition of a free volume element, the number of lattice cells (or "cubelets") belonging to a group was considered. To further approximate the value for the volume that can be occupied by the probe molecules placed on "free" grid points, (and not only the occupied part with respect to the center of the probe), a correction is made[49] for cubelets positioned at the "surface" of the FVEs.

Figure 10 shows quantitatively the shift of the size distribution between the unswollen state (*PSU*) and the swollen state (*PSU80*), which represents the system at 35 °C and 50 bar CO_2. The plot shows the fractional contribution to the *free volume* versus the radius of a volume-equivalent sphere representing the cavity size, as is common in the literature concerning PALS experiments (but in contrast to Figure 19). The bar diagrams each represent the mean value of three packing models for the respective state. Compared to the unswollen state, the swollen state shows a decrease in the number of sites of smallest volumes and an increase of medium sized and large FVEs. The area of each diagram may serve as a measure for the total accessible *free volume*. This area is larger for the swollen state, i.e., the total *free volume* increases. Because of the decreasing number of FVEs, their average size increases. This can be seen in Figure 10, where the maximum of the size distribution of the swollen state is shifted by about 2 Å to a larger value of 3−3.5 Å with respect to the radius of equivalent spheres.

CO_2 Sorption in Swollen and Unswollen Packing Models of PSU. The atomistic packing models of the swollen and unswollen state were used to calculate CO_2 sorption isotherms, assuming a rigid polymer matrix and therefore exclusively using the free volume elements of the matrix as sorption sites. This was carried out by grand canonical Monte Carlo (GCMC) simulations. This well-documented technique permits the calculation of phase equilibria between gas and sorbate phase. The properties of the sorbed CO_2 molecules in the FVEs of the polymer matrix are calculated by statistical sampling of molecular configurations that are consistent with temperature and chemical potential of the penetrants. Assuming phase equilibrium, the chemical potential is calculated from the gas phase at the specified temperature and pressure using an adequate equation of state (here: Peng Robinson).

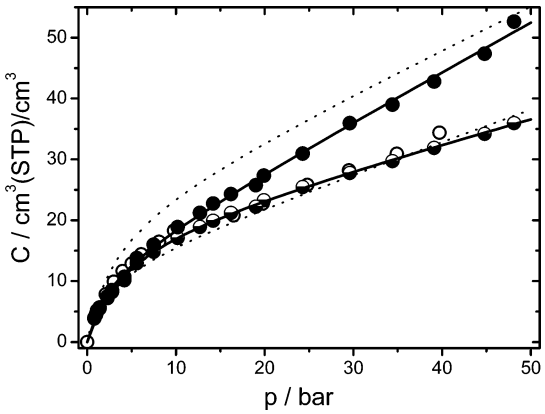

Figure 11. Sorption isotherm of CO_2 in PSU: Experimental data (●), elastic fraction of experimental data (◒), DM fits to experimental data (—), experimental data of ref 24 (○), and DM fit from ref 25, extrapolated to 50 bar (···).

Results

The application of the kinetic analysis, described in the Experimental Section, yields the fractions of mass uptake (sorption) and volume change (dilation) that follow diffusive/elastic and relaxational kinetics for each experimental step, respectively. The resulting values for each pressure step are added, resulting in two separate isotherms (diffusive/elastic and relaxational). Summation of the two parts gives the total isotherm as it is usually presented. Because a more detailed discussion of the relaxational fractions is beyond the scope of this work, here the focus is on the total isotherms and the diffusive/elastic fractions.

Sorption of CO_2 in PSU at 35 °C. *Dual Mode Sorption Analysis.* This work's sorption data of PSU/CO_2 at 35 °C are presented in Figure 11, together with the DM fit curves of Erb and Paul,[25] defining the boundaries of experimental values for PSU/CO_2 as discussed in the Introduction (see Figure 1).

The data of ref 24 are included in the plot to show that, even if the same material and the same experimental equipment is used, deviating isotherms may result, mainly due to sample prehistory but also differing analysis methods and small improvements in experimental setup. However, both isotherms lie within the range of literature data that is marked by Erb and Paul,[25] as already mentioned in the Introduction. The DM parameters of all sorption isotherms available in the literature are compiled in Table 2. The data of refs 20−26 were extracted from scanned plots and their values determined computer aided. For better comparison, least-squares fits of eq 6 (DM model) were performed with all literature data. The parameters are given in Table 2 along with the originally reported parameters, where available. As often reported and confirmed by Figure 11, the DM model is able to describe the data very well. However, the dual mode sorption parameters show a clear dependence on the maximum pressure.[55] This dependence is quite strong at pressures below 20 bar for the PSU/CO_2 system, hence it is recommended to use the parameters for interpolation only. Despite this, in Figures 1 and 11, the DM fit curves based on the data of Erb and Paul are extrapolated to 50 bar to roughly show the range of experimental data on PSU/CO_2 and to emphasize the conditioning effect that takes place during the measurement.

Figure 12 shows the dependence of the DM model parameters on the maximum pressure that is included in the fit. At a pressure of about $p_{max} = 20$ bar, the dependency levels off. Speaking in terms of the model, Langmuir mode sorption seems to be complete at this pressure, so the Henry's law solubility

Table 2. Dual Mode Sorption Parameters for PSU/CO_2 from Available Experimental Data in the Literature

			fit of eq 6 to extracted literature data			reported literature parameters		
reference	comment	p_{max} [bar]	k_d [cm^3(STP)/cm^3bar]	C_h [cm^3(STP)/cm^3]	b [1/bar]	k_d[b] [bar]	C_h' [cm^3(STP)/cm^3]	b[b] [1/bar]
Erb and Paul[25]	conditioned sample	20	0.697	21.53	0.322			
	aged sample	20	0.459	15.06	0.242			
Wang et al.[22]	as received[a]	2.5	0.724	9.683	0.594	0.383	13.3	0.396
Chiou et al.[20]	cast sample	20	0.711	19.58	0.357	0.716	19.2	0.385
	extruded sample	20	0.699	17.82	0.283	0.655	17.9	0.322
McHattie et al.[23]	cast sample	20	0.661	20.73	0.262	0.718	19.6	0.257
Wang et al.[21]	as received[a]	2.5	1.50	5.854	0.821	0.681	11.5	0.415
Kamiya et al.[26]	first sorption run	50	0.564	16.59	0.211			
	second sorption run	50	0.421	26.29	0.221			
Böhning et al.[24]	same material as this work	40	0.468	15.93	0.396	0.446	16.74	0.354

[a] The documented parameters give a best fit through the extracted data, but disagree with the parameters given by the original authors. At this low pressure range of 2.5 bar, different sets of parameter values describe the data equally well. [b] Except for ref 24, the original parameters were reported in units of cm^3(STP)/cm^3/atm and 1/atm respectively and were converted to cm^3(STP)/cm^3/bar and 1/bar using a factor of 1.01325 atm/bar.

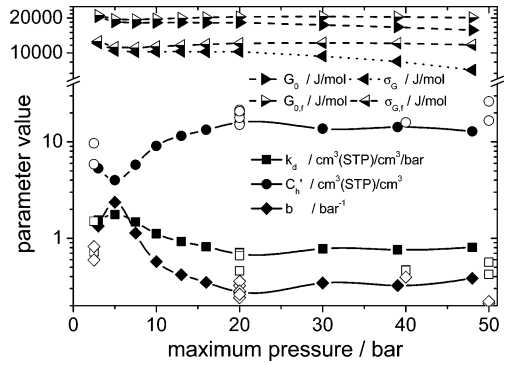

Figure 12. Dependence of model parameters on the maximum pressure used for fitting. DM parameters (■, ●, ◆), DM parameters gained from literature data (□, ○, ◇), SD parameters (left solid triangle, right solid triangle) and SD parameters of elastic fraction (half-solid left triangle, half-solid right triangle). Lines are drawn to guide the eye.

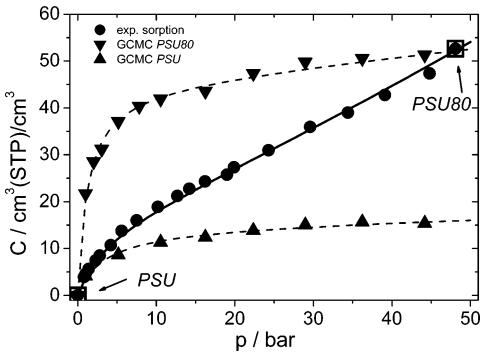

Figure 13. Sorption isotherm of CO_2 in PSU: experimental data (●), GCMC simulation on *PSU* (▲) and *PSU80* (▼), DM fits (- - -), and linear weighted average of DM fits (—) (cf. text).

koefficient k_d may be determined with reasonable certainty. Parameters of the literature data as compiled in Table 2 fit well into this scheme (open symbols).

Grand Canonical Monte Carlo (GCMC) Simulation. Sorption of gas molecules at elevated pressures is accompanied by a dilation of the polymer matrix. Because the dilation is in part relaxational, the direct molecular dynamics simulation of the processes would be too time-consuming to be realized. Therefore, Heuchel et al.[49] recently introduced the concept of using preswollen packing models to represent high concentration states of polymer/gas systems. If this approach proves to be adequate, the concept, although still dependent on experimental input, will further improve the understanding of the processes involved.

In the previous section, the packing procedure of two atomistic models of polysulfone, *PSU* and *PSU80*, was described in detail. They were built to represent the original unswollen state of polysulfone (*PSU*), and the high concentration, swollen state of the polysulfone/CO_2 system at 50 bar (*PSU80*). To verify the capability of these models to describe CO_2 solubility in polysulfone, grand canonical Monte Carlo (GCMC) simulations were performed on both packing models, in the case of *PSU80*, after removal of the 80 CO_2 molecules (models denoted as *PSU80m*). The GCMC technique allows the calculation of phase equilibria between the gas phase and the penetrant phase. The calculations were carried out on a single configurational "snapshot" of the packing models, i.e., the position of matrix atoms was fixed. The calculated concentration therefore resembles a "hole filling" without taking into account the swelling of the matrix.

This approach was used to determine concentration−pressure isotherms for both packing models with the result shown in Figure 13. Table 3 gives the parameters that best represent the calculated concentration in the swollen (*PSU80*) and unswollen (*PSU*) atomistic model, in addition to the DM parameters obtained for epxerimental data of this work. The calculated sorption isotherm for the unswollen model (*PSU*) shows good agreement to the experimental data in the low pressure range. The expected deviation at higher pressures can be understood in terms of a saturation of the above-mentioned "hole filling" process of the matrix at fixed density and accounts for the low value of the k_d parameter. Likewise, the overestimation of experimental data by the "hole filling" of the swollen model is accounted for: the *PSU80* packing model was designed to accommodate the experimental concentration of CO_2 at the indicated point (50 bar) in Figure 13 and to match its density. Therefore, its matrix is overly open at low pressures to be compared to experimental data but expectedly meets the experimental concentration at the highest pressure.

The two static reference states show good agreement only in a small pressure interval corresponding to the represented state. To overcome the disagreement between experiment and simulation at intermediate pressures, a transition between unswollen and swollen state must be achieved. The most obvious difference between *PSU* and *PSU80* are their densities. In the nonequilibrium thermodynamics of glassy polymers (NET-GP) model, introduced by Doghieri and Sarti,[15] the density of the polymer matrix is used to describe the nonequilibrium character of glassy polymer/gas systems. To predict sorption isotherms, at each pressure and given density of the matrix, the Gibbs free energy is minimized to calculate the equilibrium concentration of penetrants from pure component data. This corresponds exactly

Table 3. Dual Mode Sorption Parameters from the PSU/CO_2 Data Obtained in This Work

source	dataset/method	p_{max} [bar]	k_d [cm^3(STP)/cm^3/bar]	C_h' [cm^3(STP)/cm^3]	b [bar^{-1}]
experimental[a]	total sorption	50	0.805	12.85	0.384
	elastic fraction	50	0.390	18.49	0.238
modeling[b]	*PSU* (GCMC)	50	0.046	14.64	0.296
	PSU80 (GCMC)	50	0.171	45.07	0.813
	eq 20	50	0.865	10.78	0.450

[a] See Figure 11. [b] See Figure 13.

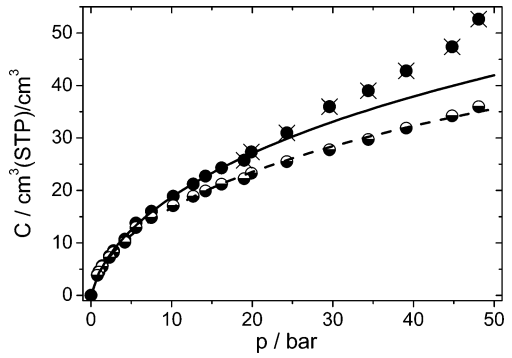

Figure 14. Sorption isotherm of CO_2 in PSU (●). Crossed out symbols were excluded from the SD fit (—). Elastic fraction: all data points (◒) are included in SD fit (- - -).

to the GCMC calculations on the *PSU* and *PSU80* model packings at the pressures 0 and 50 bar. For intermediate pressures, the assumption of a linear change in density with pressure can be adopted to accomplish the transition between *PSU* and *PSU80*. Assuming the relationship between density and solubility to be linear as well, the transition may be mathematically expressed as a linearly weighted average of both isotherms:

$$C(p) = \left(1 - \frac{p}{p_{PSU80}}\right)\cdot \bar{C}_{PSU}(p) + \frac{p}{p_{PSU80}}\cdot \bar{C}_{PSU80}(p) \quad (20)$$

where p_{PSU80} is the pressure at which *PSU80* was designed to represent the swollen state ($p = 50$ bar). $\bar{C}_{PSU}(p)$ and $\bar{C}_{PSU80}(p)$ are functions of the pressure p that best represent the calculated data points. The resulting sorption isotherm describes the experimental data rather well, as can be seen in Figure 13 and by comparison of the DM parameters listed in Table 3.

Site Distribution. Figure 14 shows the measured sorption data (total sorption) and the corresponding diffusive fraction as well as the respective representation by the site distribution model (eq 9). Following Kirchheim,[17] data above 20 bar were excluded from the fit because the model does not account for relaxational swelling of the matrix, which becomes significant at CO_2 pressures above 20 bar. Figure 12 shows also the dependence of the parameters $\hat{G}_0$ and $\hat{\sigma}_G$ of the SD model. It is obvious that the SD model parameters do not depend as strongly on the maximum pressure included in the fit as the DM model parameters do. However, if data above 20 bar are included in the fit, both parameters $\hat{G}_0$ and $\hat{\sigma}_G$ decrease slightly with increasing maximum pressure included in the fit (see Figure 12).

This result is consistent with the model: if relaxational swelling takes place, the average site volume should rise and therefore the elastic energy necessary to occupy the site decreases, hence additional sorption occurs. Also, as plasticization is progressing, i.e., the mobility of the matrix is significantly increased, stresses induced in the matrix upon gas sorption are easier to be relaxed and, as the differences in site energy lessen, the distribution of Gaussian shape decays to a Dirac delta function (one site energy for all sites). As more and more data points are included in the fit, both effects, swelling and plasticization, change the structure of the amorphous polymer matrix, and the result of the SD model fit that should give information about the original structure of the matrix is altered. In fact, the kinetic analysis indicates that relaxational swelling in the PSU/CO_2 system seems to take place at even lower pressures than 20 bar. On the other hand, the parameters that give the best fit to the data become less reliable when fewer data points are taken into account. Therefore, following the interpretation of elastic/diffusive sorption that was discussed in the Experimental Section and abiding to the supposed *origin* of the distribution of site energies as stated by eqs 7−9, it is plausible to include the diffusive fraction of sorption only to obtain the parameters of the site energy distribution. It must be noted that, even if only the diffusive fraction is taken into account, the structural changes of the matrix are taking place nonetheless, increasing the width of the site distribution. Yet, at the regarded levels of concentration, this change does not lead to significant differences in the diffusive fraction of sorption. Therefore, it is justified to utilize the complete diffusive fraction of the sorption isotherm to obtain structural information of the original matrix.

Figure 14 shows also the SD fit through the diffusive fraction of sorption. The whole set of data is represented very well. The parameters of the fit are documented in Table 4, along with best fit parameters obtained from extracted literature data, here using data below 20 bar only. The parameters obtained from data for PSU/CO_2 of Kamiya et al.[26] had been summarized by Kirchheim [17] as $\hat{G}_0 = \hat{H}_0 - T\hat{S}_0 = -16 + 0.115\cdot T$ kJ/mol before.

All values for the parameters $\hat{G}_0$ and $\hat{\sigma}_G$ of the Gaussian site energy distributions agree within 15%, with the exception of the values obtained using the number of sites $N_0 = N_{V\_connect}$ according to the *V*_connect method. To our knowledge, not many site distribution parameters for the polysulfone/CO_2 system have been published yet. However, the Gaussian parameters reported in this work are well in line with values for several polymer/CO_2 systems compiled in ref 17.

Some uncertainty remains about the number of sorption sites N_0 available to accommodate penetrant molecules. Kirchheim[17] offered several ways to estimate N_0, providing values ranging from 3×10^{21} cm^{-3} to 6×10^{21} cm^{-3}. Because none of these could be favored for physical reasons, the estimate of $N_0 = 6.7 \times 10^{21}$ cm^{-3} for easy conversion of units was applied to all polymer/gas systems.

Wang et al.[56] evaluated the Gaussian parameters independent of N_0 and used them as a fit parameter, yielding $N_0 = 1.1 \times 10^{21}$ cm^{-3} for the polycarbonate/CO_2 system, ranking at the lower limit of the estimates. On account of the comparison to the majority of published Gaussian parameters of polymer/gas systems, $N_0 = 6.7 \times 10^{21}$ cm^{-3} has been used in this work. As a matter of fact, the dependency of the Gaussian parameters and in particular of the width σ_G on the number of

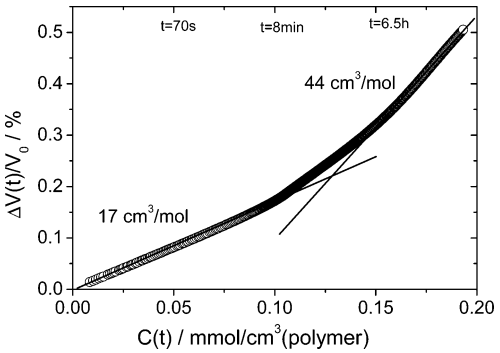

Figure 15. Dilation vs concentration of CO_2 in PSU (both time dependent) after pressure step from 25 to 30 bar (○); partial molar volumes $\tilde{V}_p$ were calculated from the slope of the curve.

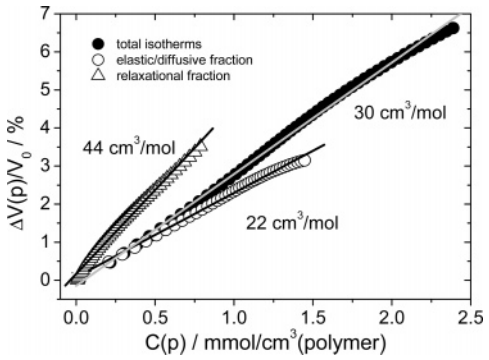

Figure 16. Dilation vs sorption of CO_2 in PSU (both pressure dependent) and the resulting partial molar volumes $\tilde{V}_p$ from the total sorption and dilation isotherms (●) as well as their diffusive/elastic (◒) and relaxational fractions (△).

sorption sites becomes quite strong toward the lower limit of N_0. It is therefore necessary to choose the number of sorption sites with great care. Using the free volume analysis of detailed atomistic packing models as described above, another basis for an estimate of the number of sorption sites is available. The corresponding results will be discussed in a later paragraph.

Dilation. *Partial Molar Volume.* Upon sorption of CO_2 molecules into the polymer matrix, a macroscopic volume change (dilation) of the polymer sample can be observed. In liquids or silicone rubbers, generally an equilibrium value of $\tilde{V}_{CO_2,rubbery} = 46$ cm³/mol is observed for the *partial* molar volume (pmv) of carbon dioxide,[4] which is close to the molar volume found for liquid CO_2. In the following, this value will be regarded as the penetrant phase molar volume ($\hat{V}_g = \tilde{V}_{CO_2,rubbery}$), as discussed above. In glassy polymers, lower values for sorbed CO_2 molecules of about 20−30 cm³/mol are reported.[12,38] For CO_2 in polysulfone (PSU), Kamiya et al.[57] report a concentration dependent pmv of 10−31 cm³/mol in the concentration interval of 5−45 cm³(STP)/cm³(polymer). Figure 15 shows the dilation of polysulfone by sorption of CO_2 following a pressure step from 25 to 30 bar. The best fits of the kinetic analysis function, eq 3, to the sorption and dilation data presented in Figures 3 and 5 were used to plot the experimentally observed dilation against the amount of CO_2 sorbed due to the current pressure step (for clarity, these fit functions were plotted as open circles). It has to be noted that the *x*-axis represents the time dependent concentration increase of CO_2. The correspondent nonlinear time scale is given at the upper *x*-axis of Figure 15. It can be seen that the pmv (i.e., the slope of the curve) is developing in time, revealing the pmv of the rapidly sorbed CO_2 (elastic/diffusive fraction) to be only 60% of that of the relaxational fraction, which turns out to be about the value for rubbery polymers or liquids $\hat{V}_g$.

As already addressed in the Introduction, Newns[19] pointed out that the initial rapid stage of sorption would lead to stresses in the polymer matrix due to the misfit ($\hat{V}_g - \hat{V}_h$) between the volume of the penetrant $\hat{V}_g$ and the volume of the sorption site $\hat{V}_h$. The relaxation of these stresses is accompanied by a decrease in chemical potential of the sorbed phase in relation to the gas phase, which is compensated by further sorption.

Using the experimentally determined partial molar volume of the rapid stage of sorption as shown in Figure 15 and the volume of the CO_2 penetrant phase $\hat{V}_g = 46$ cm³/mol, eq 19 yields an average of $\hat{V}_{h,occ} = 29$ cm³/mol for the sites occupied (index occ) in the rapid stage of sorption at this concentration level of about $C = 35$ cm³(STP)/cm³(polymer). The result of practically zero for the relaxational stage (because $\hat{V}_p \approx \hat{V}_g$) simply reflects the fact that, to accommodate a CO_2 molecule in this stage of sorption, a volume of $\hat{V}_h = \hat{V}_g$ needs to be generated by relaxation of the matrix. Figure 16 shows the pmv of CO_2 in PSU of all fractions independent of time over the whole pressure range. Polynomial fits were used to interpolate the pressure dependent data of sorption and dilation.

The values for the total isotherm (30 cm³/mol) and the elastic fraction (22 cm³/mol) lead to hole volumes of 16 and 24 cm³/mol for the average occupied sorption site, respectively. It has to be noted that the former includes the generation of additional *free volume* by relaxation and therefore misrepresents the average size of occupied sorption sites because eq 19 only considers elastic deformation, which is represented by the value obtained from the elastic fraction.

Partial Molar Volume from MD Simulations. The effect of volume dilation of a polymer by sorption of CO_2 can also be observed and analyzed utilizing molecular dynamics simulations. Because simulation of the diffusion of carbon dioxide into the packing model is far too time-consuming, the penetrant molecules are inserted into the packing model with a Monte Carlo procedure so that a configuration of minimal energy is obtained. In this case, $N = 24$ molecules were inserted into a single unswollen packing model (*PSU*), corresponding to a concentration of 15.6 cm³(STP)/cm³(polymer). A short *NVT* MD run of a few femtoseconds is at first needed to energetically stabilize the system after the insertion of penetrants into arbitrary positions. The system is then allowed to reach a (pseudo-) equilibrium volume performing an *NpT*-MD run of 300 ps at $p = 10$ bar and $T = 308$ K. Concentration, pressure, and temperature parameters for this MD simulation were chosen according to the mass uptake of CO_2 into polysulfone in a one-step sorption experiment (0−10 bar at 308 K).

Figure 17a shows the resulting volume dilation average of three packing models. The near instantaneous "reaction" of the models even on this small time scale and the partial reversability upon removal of the penetrants point to the elastic character of the dilation. The hysteresis that shows up in the contraction suggests that part of the induced dilation requires more time to recover. It must be noted that the individual packing models behave differently in this regard, one recovering completely while the other two showed significant hysteresis. It stands to reason that contraction upon removal of penetrants shows some inelastic behavior because penetrant molecules surely produce a stronger driving force than missing penetrants. In fact, longer runs of penetrant filled packing models showed some small additional dilation behavior on the time scale of a nanosecond.

In the corresponding laboratory experiments, sorption as well as dilation (see Figure 17b), the CO_2 pressure is raised in a single step from $p = 0$ bar to $p = 10$ bar and released again after 2 h. In the sorption measurement, a (pseudo-) equilibrium

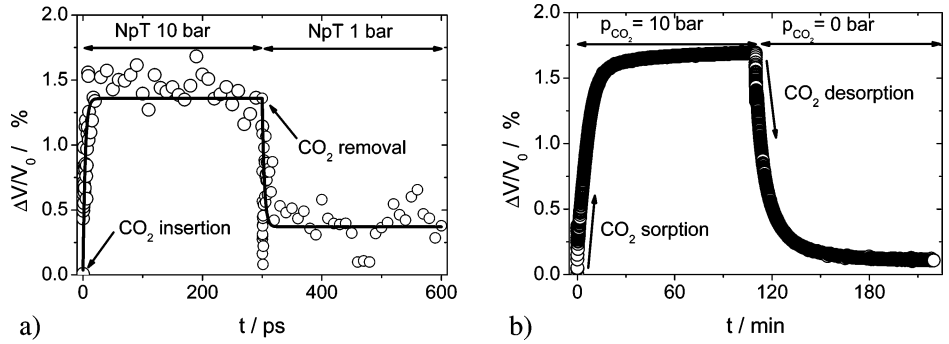

Figure 17. Dilation and contraction after insertion/removal of CO_2 molecules into PSU packing model and subsequent equilibration (*NpT*-MD) (a), and following a pressure step from 0 to 10 bar in a laboratory experiment (b). The solid line in (a) is drawn to guide the eye.

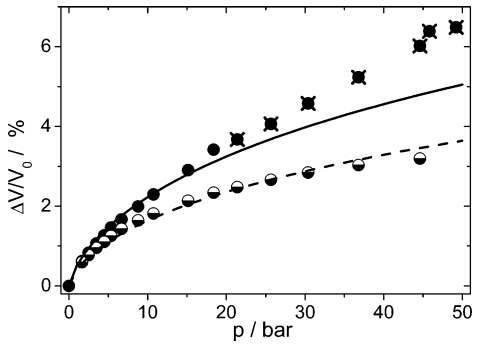

Figure 18. Experimental dilation (●) and its elastic fraction (◒). The solid line represents a best fit of the average hole volume $\hat{V}_{h0}$ to the total dilation (crossed out symbols excluded) and the dashed line to the elastic fraction (all points included), in each case using the respective parameters $\hat{G}_0$ and $\hat{\sigma}_G$ obtained from the sorption fit.

concentration of 15.6 cm^3(STP)/cm^3(polymer) was reached. Simultaneous to the sorption/desorption of CO_2, which is following Fickian diffusion kinetics, the polymer sample shows almost reversible dilation and contraction. The slight hysteresis that is observed in the contraction can be ascribed to the concentration dependence of the diffusion coefficient and of the mobility of the polymer matrix and should therefore not be related to the above-mentioned hysteresis of the simulated dilation, which is expected to recover on a much smaller time scale.

The agreement in sorptive dilation of experiment and model within 20% is remarkable, considering the small size of the packing models and the fact that on this small time scale, no substantial diffusive jumps are observed and therefore the contribution to the overall dilation in a laboratory experiment, caused by CO_2 molecules present in diffusion paths, cannot be represented by MD simulation without the consumption of more CPU time by orders of magnitude.

The calculated partial molar volume for the simulated dilation of PSU by CO_2 amounts to 19 cm^3/mol, while the actual experiment finds 24 cm^3/mol, indicating occupied holes of an average volume of 27 and 22 cm^3/mol, respectively (eq 19).

Volume Distribution of Sorption Sites. In the context of the site distribution model, the local volume fluctuations of Gaussian form at temperatures above T_g are frozen in at lower temperatures and lead to a size distribution of hole volumes, which again leads to the Gaussian distribution of site energies with the average site energy $\hat{G}_0$ and width $\hat{\sigma}_G$. The parameters can be gained from a fit of eq 11 to a sorption isotherm. Once the parameters are known, eq 12 can be fitted to a dilation isotherm adjusting the average hole volume $\hat{V}_{h0}$, while the width $\hat{\sigma}_V$ of the volume distribution is derived from eq 10 using $\hat{\sigma}_G$.

Figure 18 shows the result of the fits to the total dilation (solid line), again not including data above 20 bar, and to the elastic fraction data (dashed line). The resulting parameters are compiled in Table 4. Again, as explained in the former paragraph, it is plausible to use the data and parameters of the elastic fraction, which are expected to give the best representation of the structure of the original matrix.

As pointed out earlier in this work, the choice of the number of sorption sites $N_0 = 6.7 \times 10^{21}$ cm^{-3}, to be used in eqs 8 and 9 of the SD model, has been a matter of rough estimates. Ultimately, the value of $N_0 = 6.7 \times 10^{21}$ cm^{-3} was chosen for

Table 4. Site Distribution (SD) Model Parameters (eqs 11 and 12) of Experimental Data[a] for PSU/CO_2 of This Work and Literature Data and Number and Average Volume of FVEs as Determined from Atomistic Packing Models

		Gaussian site energy distribution		Gaussian size distribution of spherical holes		number of sites
		$\hat{G}_0$ [kJ/mol]	$\hat{\sigma}_G$ [kJ/mol]	$\hat{V}_{h0}$ [cm^3/mol][e]	$\hat{\sigma}_V$ [cm^3/mol][e]	N_0 [10^{21} cm^{-3}]
Erb and Paul[25]	aged	20.7	11.9			6.7
	conditioned	18.1	11.4			6.7
Wang et al.[22]		19.2	11.0	20.4	6.2	6.7
Kamiya et al.[26]	35 °C	19.0[b]	12.1[b]			6.7
	45 °C	20.2[d]	12.1[d]			6.7
	55 °C	21.1[d]	12.1[d]			6.7
	65 °C	21.9[d]	12.1[d]			6.7
total isotherm (<20 bar)		18.2	10.2	16.2	3.4	6.7
elastic fraction		20.1	11.8	18.2	5.0	6.7
$N_0 = N_{V\_connect}$		12.9	8.0	20.7	4.7	2.8
$N_0 = N_{R\_max}$		17.5	10.6	19.0	5.0	4.9
PSU/*V*_connect				35.0[c]		2.8
PSU/*R*_max				19.0[c]		4.9

[a] If not stated otherwise, parameters refer to measurements at 35 °C. [b] Second sorption run at 35 °C. [c] Average value from three packing models. [d] Width of the distribution was held fixed and only $\hat{G}_0$ was varied to fit the data. [e] Use a factor of 1.66 $Å^3$/(cm^3/mol) to convert into $Å^3$.

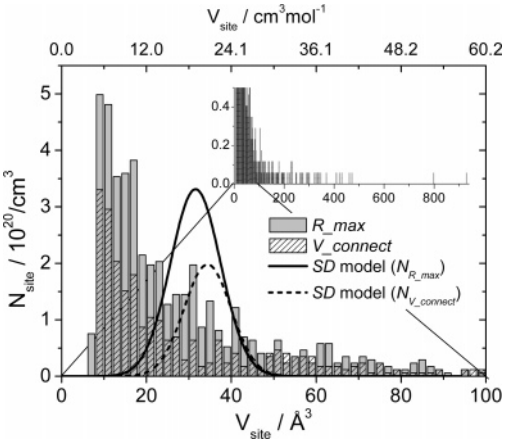

Figure 19. Site distribution as probed directly in the packing model (*PSU*) and calculated from experimentally obtained *SD* parameters using N_{V_connect} and N_{R_max} as number of sorption sites N_0 (see eqs 8 and 9).

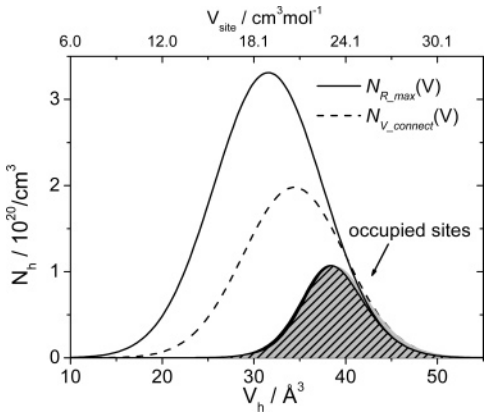

Figure 20. Hole-size distributions according to the *SD* model obtained from experimental data, using the number of available sorption sites from *free volume* analysis of packing models (solid line: *R*_max and dashed line *V*_connect method). The hatched area represents the coinciding occupied sites at a concentration level of 35 cm³(STP)/cm³. It can be seen that, in this range, the distribution of occupied sites is practically independent of the analysis method of FVE.

convenient unit conversion. The free volume analysis of the static packing models discloses a possibility of determination of the number of sorption sites. Two methods were introduced in a previous section that probe the free volume distribution of atomistic packing models. The analysis was performed on three independent unswollen models of polysulfone (PSU). Both methods of analysis, *R*_max and *V*_connect, depend on the choice of probe and grid size; while the former will find more and smaller sites with decreasing parameters because the nonaccessible volumes (e.g., within phenylene rings) are detected as well, the latter method will eventually detect the complete free volume as one space. To reasonably deal with the problem, the probe size was set to the size of a hydrogen atom (van der Waals radius), with about half the radius as grid spacing. It is inherent in the method of analysis to exhibit the greatest uncertainties for small volumes where the dimensions of the volume are comparable to the grid spacing. Furthermore, it is an artifact of the calculation algorithm to yield undersized volumes if the number of free grid points is small. Therefore, for the determination of the number of sorption sites, all spaces of volumes not larger than that of hydrogen were assumed to be "bottlenecks" (potential diffusion paths) rather than sorption sites and excluded. This appears somewhat arbitrary, but Figure 19 shows that this specification leads to reasonable results concerning the comparison to distributions gained by the site distribution model.

Both distributions obtained this way are displayed as bar charts in Figure 19. As expected, the *R*_max method yields more but smaller sites ($N_{R\_\text{max}} = 4.9 \times 10^{21}$ cm^{-3}, $\hat{V}_h = 19$ cm^3 mol^{-1}), whereas the *V*_connect method detects a number of very large free volume elements ($N_{V\_\text{connect}} = 2.8 \times 10^{21}$ cm^{-3}, $\hat{V}_h = 35$ cm^3 mol^{-1}). These modeling results for the number of sites agree very well with the estimates of Kirchheim, and therefore such packing models seem to be an alternative source for the determination of this parameter.

The total number of sites per packing model of each method was taken as parameter N_0 to fit the SD model (eq 12) to experimental data. Parameters and results of the obtained hole size distributions are compiled in Table 4 and shown in Figure 19. It should be noted that both Gaussian distributions coincide at the large volume tail. This is expected because in this way, up to the concentration level reached in the experiment, the same dilation effect is achieved regardless of the number of sorption sites. In Figure 20, this is demonstrated by showing the Gaussian distributions presented in Figure 19 along with the distribution of occupied sites. To obtain the latter, the distributions of site volumes $N_{R\_\text{max}}(V_h)$ and $N_{V\_\text{connect}}(V_h)$ were multiplied with a Fermi−Dirac statistic of a width σ_{FD} scaled in the same manner as the widths $\hat{\sigma}_V$ to $\hat{\sigma}_G$. The area under the distributions of occupied sites represent the concentration level of the diffusive fraction at 45 bar. In the hatched area, the distributions of occupied sites of both site volume distributions $N_{V\_\text{connect}}(V_h)$ and $N_{R\_\text{max}}(V_h)$ coincide, differing only in the upper and lower volume margin (black: *R*_max; gray: *V*_connect).

It is comprehensible that, within limits, any number of sorption sites N_0 will result in a Gaussian distribution that

Table 5. Obtained Values for the Partial Molar Volumes of CO_2 in PSU[a] and the Occupied Hole Size According to eq 19

reference	method[b]	comment	$\tilde{V}_p$ [cm³/mol][c]	$\hat{V}_{h,occ}$ [cm³/mol][c]
Fleming et al.[4]	CO_2 in liquids	6-liquid-average	46	
Kamiya et al.[57]	concentration dependent	5−45 cm³/cm³ range	10−31	36−15
this work	time dependent	rapid stage	17	29
		relaxational stage	44	
	pressure dependent	total isotherms	30	16
		elastic fraction	22	24
		relaxational fraction	44	
	NpT-MD simulation		13	33
	interval step	elastic fraction	31	15
	site distribution model		21	25
	*R*_max		- -	48

[a] Except for ref 4, which is reported to give a measure of a truly relaxed pmv of sorbed CO_2. [b] All values were determined at 35 °C. [c] Use a factor of 1.66 Å³/(cm³/mol) to convert to Å³.

coincides with the large volume tail of another and yield an equally good fit to the data. Accordingly, the mean volume V_{h0} as well as the width $\hat{\sigma}_V$ will decrease with an increasing number of sites. For the comparison of the Gaussian distributions with those found by analysis of atomistic packing models, it also has to be kept in mind that, while the SD model is derived from considerations of the above-T_g dynamics, the volume analysis is performed on a static atomistic model of polysulfone. Moreover, continuum mechanics and idealized spherical shapes are assumed in the SD model, whereas the volumetric analysis does not distinguish between geometrical shapes. But large volumes detected by model analysis may well be narrow in one or two dimensions and not necessarily accommodate penetrant molecules as well as would spherical holes of the same volume. This will especially be the case for the *V*_connect method. Despite these potential drawbacks, volumes are found within the same order of magnitude. In fact, the mean volume of sites of the *R*_max method even matches that of the corresponding Gaussian distribution of the SD model.

At a CO_2 concentration of 35 cm^3(STP)/cm^3(polymer), which corresponds to the concentration of the elastic fraction at 45 bar, about 20% of the sites (*R*_max) are occupied. Filling up the sites of a Gaussian distribution to that level from the largest to the smallest hole, the average occupied hole has a volume of 25 cm^3/mol (see upper axis of Figure 19); applying the same procedure to the *R*_max distribution yields 49 cm^3/mol. But while for the Gaussian distribution this yields a partial molar volume of 21 cm^3/mol that agrees well with the other values in Table 5, the average volume of the *R*_max distribution, pictured as a spherical hole, would be large enough to accommodate CO_2 penetrant molecules without dilation. This is another argument to incorporate the dynamics and aspherical geometries in a more detailed, general analysis of the intermolecular space of polymer packing models with regard to the assessment of possible sorption sites.

Conclusions

Several aspects of the sorption of CO_2 in polysulfone and the thereby induced swelling behavior were investigated experimentally and by detailed atomistic molecular modeling. Utilizing a viscoelastic model, the experimentally observed process of sorptive dilation could consistently be separated into a diffusive/elastic part and a relaxational part by kinetic analysis. While the nearly instantaneous elastic response of the polysulfone matrix to penetrating CO_2 could be reproduced by detailed atomistic MD simulations with success, the resulting relaxational behavior is observed on experimental time scales that are orders of magnitudes too long to directly simulate the respective molecular dynamics in reasonable time and effort. However, the investigation of atomistic packing models of swollen "reference states" partially overcomes this gap, and it is shown that the combination of two reference states is well able to describe intermediate states of the sorption isotherm. This agreement validates both the general approach and the quality of the molecular models.

In addition, the *free volume* of the detailed atomistic packing models was analyzed and the size distribution was compared to the results of the analysis of experimental data according to the site distribution model. The kinetic analysis and consistent implementation of its results, i.e., the exclusive usage of the elastic fraction, improved the quality and reliability of the resulting model parameters. Reasonably agreeing size distributions of sorption sites were obtained experimentally and by analysis of molecular models, even though some open questions remain regarding the shape of the distribution.

The fact that the site distribution model is able to describe the diffusive/elastic fraction of experimental sorption and dilation data quite well and the reasonable agreement of the parameters with modeling results, in unison with the successful simulation of the elastic response of the matrix to penetrant molecules by detailed atomistic modeling, confirms, to a certain extent, the perception of the processes involved as established by the site distribution model.

Following up on these promising new ways of comparison of laboratory experiments and molecular modeling, further effort is necessary to converge the respective boundary conditions and to reconcile them with the assumptions made by phenomenological models.

Appendix

Selected Notations Used in This Work

$\hat{V}_i$	molar volume of species *i*
V_i	volume of species *i*
$\hat{N}_i$	molar quantity of species *i*
ΔV	volume change of the polymer/gas system
$\Delta\hat{N}_i$	change of molar quantity of species *i*
$\tilde{V}_i = \Delta V/\Delta\hat{N}_i$	partial molar volume of species *i*
$\hat{V}_{g,i}$	"penetrant phase" molar volume of species *i* in relaxed environment
$\hat{V}_g$	molar volume of CO_2 (gas) solved in liquids (relaxed environment)
$\hat{V}_h$	(spherical) volume of a sorption site (hole)
$\hat{V}_{h,occ}$	molar volume of occupied sites (average)
$\tilde{V}_p$	partial molar volume of CO_2 (penetrant)
N_0	number of sorption sites per volume unit of polymer (ref 17)
$N_{V\_connect}$	number of FVEs detected by the *V*_connect method
N_{R_max}	number of FVEs detected by the *R*_max method

Acknowledgment. We thank Dieter Hofmann, GKSS, for inspiring discussions and the Deutsche Forschungsgemeinschaft for financial support under contracts Bo1921/1-1 and He2108/2-1.

References and Notes

(1) Tomasko, D. L.; Li, H.; Liu, D.; Han, X.; Wingert, M. J.; Lee, L. J.; Koelling, K. W. *Ind. Eng. Chem. Res.* **2003**, *42*, 6431−6456.
(2) Ismail, A. F.; Lorna, W. *Sep. Purif. Technol.* **2002**, *27*, 173−194.
(3) Hofmann, D.; Fritz, L.; Ulbrich, J.; Schepers, C.; Böhning, M. *Macromol. Theory Simul.* **2000**, *9*, 293−327.
(4) Fleming, G. K.; Koros, W. J. *Macromolecules* **1986**, *19*, 2285−2291.
(5) Paul, D. R. *Ber. Bunsen-Ges. Phys. Chem.* **1979**, *83*, 294−302.
(6) Weiss, G. H.; Bendler, J. T.; Shlesinger, M. *Macromolecules* **1992**, *25*, 990−992.
(7) Jordan, S. S.; Koros, W. J. *Macromolecules* **1995**, *28*, 2228−2235.
(8) Paterson, R.; Yampol'skii, J.; Fogg, P. G. T. *J. Phys. Chem. Ref. Data* **1999**, *28*, 1255−1450.
(9) Vrentas, J. S.; Vrentas, C. M. *Macromolecules* **1991**, *24*, 2404−2412.
(10) Lipscomb, G. G. *AIChe J.* **1990**, *36*, 1505−1516.
(11) Raucher, D.; Sefcik, M. D. *ACS Symp. Ser.* **1983**, *223*, 111−124.
(12) Mi, Y.; Zhou, S. Stern, S. A. *Macromolecules* **1991**, *24*, 2361−2367.
(13) Wissinger, R. G.; Paulaitis, M. E. *Ind. Eng. Chem. Res.* **1991**, *30*, 842−851.
(14) Conforti, R. M.; Barbari, T. A.; Vimalchand, P.; Donohue, M. D. *Macromolecules* **1991**, *24*, 3388−3394.
(15) Doghieri, F.; Sarti, G. C. *Macromolecules* **1996**, *29*, 7885−7896.
(16) Sanchez, I. C.; Lacombe, R. H. *Macromolecules* **1978**, *11*, 1145−1156.
(17) Kirchheim, R. *Macromolecules* **1992**, *25*, 6952−6960.
(18) Kirchheim, R. *J. Polym. Sci., Part B: Polym. Phys.* **1993**, *31*, 1373−1382.
(19) Newns, A. C. *Trans. Faraday Soc.* **1956**, *52*, 1533−1545.

(20) Chiou, J. S.; Maeda, Y.; Paul, D. R. *J. Appl. Polym. Sci.* **1987**, *33*, 1823−1828.
(21) Wang, J. S.; Kamyia, Y.; Naito, Y. *J. Polym. Sci., Part B: Polym. Phys.* **1998**, *36*, 1695−1702.
(22) Wang, J. S.; Kamyia, Y. *J. Membr. Sci.* **1995**, *98*, 69−76.
(23) McHattie, J. S.; Koros, W. J.; Paul, D. R. *Polymer* **1991**, *32*, 840−850.
(24) Böhning, M. Untersuchungen der Gaspermeationseigenschaften von Polymeren und dabei auftretender Wechselwirkungs- und Quellungsphänomene. Ph.D. Thesis, Technical University of Berlin, Wissenschaft und Technik Verlag: Berlin, 1997.
(25) Erb, A. J.; Paul, D. R. *J. Membr. Sci.* **1981**, *8*, 11−22.
(26) Kamiya, Y.; Hirose, T.; Mizoguchi, K.; Naito, Y. *J. Polym. Sci., Part B: Polym. Phys.* **1986**, *24*, 1525−1539.
(27) Wissinger, R. G.; Paulaitis, M. E. *J. Polym. Sci., Part B: Polym. Phys.* **1987**, *25*, 2497−2510.
(28) Hirose, T.; Mizoguchi, K.; Kamiya, Y. *J. Polym. Sci., Part B: Polym. Phys.* **1986**, *24*, 2107−2115.
(29) Kamiya, Y.; Naito, Y.; Terada, K.; Mizoguchi, K.; Tsuboi, A. *Macromolecules* **2000**, *33*, 3111−3119.
(30) Shenoy, S.; Woerdeman, D.; Sebra, R. Garach-Domech, A.; Wynne, K. J. *Macromol. Rapid Commun.* **2002**, *23*, 1130−1133.
(31) Wind, J. D.; Sirard, S. M.; Paul, D. R.; Green, P. F.; Johnston, K. P.; Koros, W. J. *Macromolecules* **2003**, *36*, 6433−6441.
(32) Liu, D.; Li, H.; Noon, M. S.; Tomasko, D. L. *Macromolecules* **2005**, *38*, 4416−4424.
(33) Böhning, M.; Springer, J. *Polymer* **1998**, *39*, 5183−5195.
(34) Crank, J. *The Mathematics of Diffusion*, 2nd ed.; Oxford Science Publications: New York, 1975.
(35) Berens, A. R.; Hopfenberg, H. B. *Polymer* **1978**, *19*, 489−496.
(36) Wessling, M.; Huisman, I.; van der Boomgard, T.; Smolders, C. A. *J. Polym. Sci., Part B: Polym. Phys.* **1995**, *33*, 1371−1384.
(37) Sperling, L. H. *Introduction to Physical Polymer Science*; Wiley-Interscience: New York, 2001.
(38) Gotthardt, P.; Grüger, A.; Brion, H. G.; Plaetschke, R.; Kirchheim, R. *Macromolecules* **1997**, *30*, 8058−8065.
(39) Punsalan, D. T. A Sorption and Dilation Investigation of Amorphous Glassy Polymers and Physical Aging. Ph.D. Thesis. University of Texas at Austin, 2001.
(40) Eshelby, J. D. In *Solid State Physics*; Seitz, F., Turnbull D., Eds.; Academic Press: New York 1956.
(41) Theodorou, D. N.; Suter, U. W. *Macromolecules* **1985**, *18*, 1467−1478.
(42) Theodorou, D. N.; Suter, U. W. *Macromolecules* **1986**, *19*, 139−154.
(43) *Polymer User Guide, Amorphous Cell Section*, version 4.0.0p+; Molecular Simulations Inc.: San Diego, CA, 1999.
(44) Sun, H.; Rigby, D. *Spectrochim. Acta, Part A* **1997**, *53*, 1301−1323.
(45) Rigby, D.; Sun, H.; Eichinger, B. E. *Polym. Int.* **1997**, *44*, 311−330.
(46) Gusev, A. A.; Suter U. W. *Phys. Rev. A* **1991**, *43*, 6488−6494.
(47) Gusev, A. A.; Arizzi, S.; Suter, U. W.; Moll D. J. *J. Chem. Phys.* **1993**, *99*, 2221−2227.
(48) Gusev, A. A.; Suter U. W. *J. Chem. Phys.* **1993**, *99*, 2228−2234.
(49) Heuchel, M.; Böhning, M.; Hölck, O.; Siegert, M. R.; Hofmann, D. *J. Polym. Sci., Part B: Polym. Phys.* **2006**, *44*, 1874−1897.
(50) Hofmann, D.; Heuchel, M.; Yampolskii, Yu.; Khotimskii, V.; Shantarovich, V. *Macromolecules* **2002**, *35*, 2129−2140.
(51) Heuchel, M.; Hofmann, D.; Pullumbi, P. *Macromolecules* **2004**, *37*, 201−214.
(52) Malhotra, B. D.; Pethrick, R. A. *Eur. Polym. J.* **1983**, *19*, 457−459.
(53) Yuan, J.-P.; Cao H.; Hellmuth, E. W.; Jean, Y. C. *J. Polym. Sci., Part B: Polym. Phys.* **1998**, *36*, 3049−3056.
(54) Bohlen, J.; Wolff, J.; Kirchheim, R. *Macromolecules* **1999**, *32*, 3766−3773.
(55) Bondar, V. I.; Kamiya, Y.; Yampol'skii, Y. P. *J. Polym. Sci., Part B: Polym. Phys.* **1996**, *34*, 369−378.
(56) Wang, J. S.; Kamiya, Y. *J. Polym. Sci., Part B: Polym. Phys.* **2000**, *38*, 883−888.
(57) Kamiya, Y.; Hirose, T.; Naito, Y.; Mizoguchi, K. *J. Polym. Sci., Part B: Polym. Phys.* **1988**, *26*, 159−177.

MA061562R